Structure-Based Design of Potent Histatin Analogues[†]

Dyanne Brewer and Gilles Lajoie*

Guelph-Waterloo Centre for Graduate Work in Chemistry and Biochemistry, Department of Chemistry, University of Waterloo, Waterloo, Ontario N2L 3G1, Canada

Received November 9, 2001; Revised Manuscript Received February 19, 2002

ABSTRACT: Conformational studies of human salivary peptide, histatin 3 (Hst3), were performed by nuclear magnetic resonance (NMR) and circular dichroism (CD) spectroscopy in a membrane-mimicking environment. The structural information that was obtained was used in the design of peptide analogues with improved antifungal activity. In the presence of increasing concentrations of L-α-dimyristoylphosphatidylcholine (L-α-DMPC) lipid vesicles, a dramatic increase in a minimum at 198 nm is observed in the CD spectra of Hst3. The NMR data of Hst3 in the presence of L-α-DMPC lipid vesicles reveal the proximity of residues Y^{10} and S^{20}, indicating the existence of a more compact structure. Peptide analogues were designed on the basis of this observation, which incorporated a disulfide bond to stabilize an extended loop in this region of the sequence. One of these, peptide 4, was 100 times more potent than Hst5 against *Saccharomyces cerevisiae* cells. Conformational analysis of peptide 4 revealed a looped structure with charged residues protruding on the outside surface, while a combination of aromatic residues and histidines are packed into an internal core.

Histatins are a family of multifunctional histidine-rich peptides found in human saliva (*1*). They have potent antibacterial and antifungal activity, thus contributing to the host nonimmune defense system (*2*). Histatins are members of a larger group of naturally occurring antimicrobial peptides. Numerous and varied types of antimicrobial peptides have been isolated from plants, amphibians, mammals, bacteria, and fungi (*3*). The higher organisms synthesize these peptides by standard ribosomal machinery to play an essential role in nonspecific host defense. Peptides with potent activity against fungi but not lethal to mammalian cells are of particular interest due to the increasing number of patients at risk for invasive fungal infections as well as the development of fungal resistance to and the toxicity of current treatments (*4*). Histatins have significant activity against *Candida albicans* (*2*), which is an opportunistic pathogenic fungus. Investigations into the mechanism of action of peptides like the histatins can provide information into innate immunity and potential new strategies for antifungal therapy.

Histatins are secreted by the parotid and submandibular glands but have also been detected in human plasma at lower concentrations (*5*, *6*). There are 12 peptides in the histatin family; two of the major histatins are histatin 3 (Hst3)[1] and histatin 5 (Hst5). Hst5 is either a proteolytic degradation product of Hst3 or a post-transcriptional modification of Hst3 mRNA (*7*). Hst3 has a sequence of 32 amino acids, and Hst5 contains 24 amino acids (Table 2). Histatins contain a large number of basic residues, including seven histidines.

In addition to their antimicrobial activities, histatins possess several other diverse biological properties such as playing an important role in the maintenance of oral fluids (*8*). Hst5 has also been shown to act synergistically with epidermal growth factor (EGF) to promote rabbit chondrocyte proliferation (*6*), suggesting possible applications of these peptides in wound healing. The application of histatins for bone and peridontal tissue regeneration has also been investigated (*9*, *10*).

Histatins, unlike several other antimicrobial peptides (*11*), do not possess amphipathic character. Their mechanism of action appears to be distinct from those of other antimicrobial peptides but is still unclear. A putative Hst5 binding protein has been isolated from the cell membrane of both *C. albicans* and *Saccharomyces cerevisiae* cells, and Hst5 binding to this protein has been correlated to the killing of *C. albicans* cells (*12*). A form of fluorescently labeled Hst5 was found to be internalized into *C. albicans* cells and suggested to target the energized mitochondrion (*13*). It has also been recently reported that mitochondrial ATP synthesis is required for effective killing of *C. albicans* cells by Hst5 (*14*) and that ATP released extracellularly is a cytotoxic mediator of killing (*15*, *16*). Fluorescently labeled Hst3 has also been found to penetrate *C. albicans* cells, although an internal target was not identified (*17*).

Previous conformational analysis of histatin peptides has focused on either the C-terminal 16-residue fragment of Hst5 or on Hst5 itself (*18*−*20*). Hst5 was reported to have a random coil structure in aqueous solution at pH 3.8 and to become entirely helical in DMSO (*19*). CD studies of Hst5

[†] D.B. was a recipient of an NSERC graduate scholarship.

* To whom correspondence should be addressed: Department of Biochemistry, University of Western Ontario, London ON N6A 5C1, Canada. Phone: (519) 663-3054. Fax: (519) 663-2936. E-mail: glajoie@uwo.ca.

[1] Abbreviations: CD, circular dichroism; Hst3, histatin 3; Hst5, histatin 5; NOESY, nuclear Overhauser effect spectroscopy; TFE, trifluoroethanol; TOCSY, total correlation spectroscopy; HPLC, high-performance liquid chromatography; NMR, nuclear magnetic resonance; ESI-MS, electrospray ionization mass spectrometry; TFA, trifluoroacetic acid; L-α-DMPC, L-α-dimyristoylphosphatidylcholine; MIC, minimum inhibitory concentration; UV, ultraviolet; DMSO, dimethyl sulfoxide; SDA, Sabourand dextrose agar; NOE, nuclear Overhauser effect.

10.1021/bi015926d CCC: $22.00
Published on Web 04/06/2002

in the presence of zinc ions and negatively charged membrane vesicles have indicated an α-helical secondary structure for the peptide (*20*). There is contradictory evidence with respect to whether the tendency to form an α-helix is functionally important (*18*, *21*−*23*). NMR studies in 90% trifluoroethanol at pH 3.6 revealed that Hst5 has two helical tracts with a break in secondary structure between residues G^9 and K^{11} (*20*). From these studies, it was proposed that the antifungal activity of Hst5 requires a conformational change that results from the interaction of the peptide with both zinc ions and biological membranes (*20*).

In a previous study from our group, the conformations of Hst3 and Hst5 were examined in aqueous and nonaqueous solutions by CD and NMR (*24*). CD analysis of Hst3 determined that Hst3 did not have well-defined secondary structure in aqueous solution at pH 7.4 (*24*). However, unlike the case for Hst5, the addition of TFE reduced its secondary structural content (*24*). NMR analysis of Hst3 in aqueous solution revealed a turn or loop structure in the middle of the sequence as well as a C-terminal helix, which are stabilized in mixed aqueous/organic environments but destabilized in pure DMSO (*24*). The turn or loop structure in the middle of the sequence may correspond to the break in the helical tracts found by Melino and co-workers (*20*) in Hst5. These NMR results suggested a less conformationally flexible structure for the longer Hst3 peptide than for Hst5.

Our goal was to obtain conformational information about Hst3 and use it in the design of improved antifungal peptides. In this paper, we report our investigation of the conformation of Hst3 by performing CD and NMR analysis of the peptide in the presence of L-α-dimyristoylphosphatidylcholine (L-α-DMPC) lipid vesicles to assess its behavior in membrane-like environments. Long-range interactions were observed which suggested a folded or more compact structure for Hst3 where residues 10 and 20 are close to each other under these conditions. This observation was then used as the basis for the design of a cyclic analogue prepared by the incorporation of a disulfide bond. The first analogue was designed to place the disulfide bridge near the region containing the long-range interaction detected in the NMR experiments. In addition, it was thought that replacing the two glycines at positions 9 and 23 would have a minimal effect on the structure or antifungal properties. Several other peptides were made by varying the placement of the disulfide bridge, and each was tested for antifungal activity. Peptide 4 which had the most improved antifungal activity, compared to Hst5, was then analyzed by NMR and CD spectroscopy in various environments.

EXPERIMENTAL PROCEDURES

Peptide Synthesis and Purification

All peptides were prepared using Fmoc chemistry on a Milligen 9050 continuous flow solid-phase peptide synthesizer with 1-hydroxybenzotriazole (HOBt) and benzotriazol-1-yloxytris(dimethylamino)phosphonium hexafluorophosphate (BOP) as coupling reagents (*25*). Peptides were assembled on Wang resin (*26*). The side chains of serine, tyrosine, and glutamic and aspartic acid were protected with the *tert*-butyl group. Arginine was protected with pentamethylchromane-6-sulfonyl (PMC). Histidine and cysteine were protected with the trityl group, and lysine was protected as the *tert*-butyloxycarbonyl group (Boc). The side chain of asparagine was protected as the *N*-trityl group to minimize dehydration. In cases where orthogonal protection was required, glutamic acid was protected with the allyl group and lysine with the allyloxycarbonyl group (Aloc). Peptides were cleaved from the support according to the procedure of Sole and Barany (*27*). Disulfide bond formation was achieved via air oxidation of the free linear crude peptide (0.5 mg/mL) in a 0.1 M deaerated solution of ammonium bicarbonate (*28*). Cyclization via amide bond formation was achieved through the orthogonal protection of a lysine and glutamic acid residue with Aloc and allyl protecting groups at positions 4 and 15, respectively. Selective removal of these side chain protecting groups was achieved under mild conditions with a Pd(0) catalyst while the peptide remained attached to the resin and the other side chains remained protected (*29*). After this removal, an amide bond was formed between the side chains using benzotriazol-1-yloxytris(pyrrolidino)phosphonium hexafluorophosphate (pyBop) and HOBt as coupling reagents (*30*).

Crude yields of all analogues were better than 75%. Peptides were purified by reversed phase HPLC using a semipreparative C-18 Zorbax (Waters) column with a gradient of 5 to 95% acetonitrile containing 0.1% TFA. The identity and purity of all peptides were determined by ESI-MS on a Quattro II mass spectrometer (Micromass). The purity was also determined to be at least 95% by analytical HPLC.

Antifungal Activity

The fungistatic assay employed in this study was developed by Gordon and co-workers to test azole antifungal drugs (*31*). This method involves the use of a pH-controlled semisolid medium and standardized inoculum. The advantage of this assay is that the medium is simple to prepare and has a relatively long refrigerator shelf life in a ready-to-use state. The fungistatic drug ketoconazole was used as a positive control in all of our assays. Furthermore, when histatin analogues were tested, Hst3 and/or Hst5 was used as a positive peptide control. The minimum inhibitory concentration (MIC) was used as a quantitation factor for antifungal activity (*32*).

Stock peptide solutions (600 μL or 1 mL) at a concentration 10 times greater than the final concentration of the most concentrated test sample in a sodium phosphate buffer (0.01 M, pH 7.4) were prepared. The peptide concentration was determined by the UV absorbance at a λ of 275 nm [tyrosine $\epsilon = 1390$ in H_2O (*33*)]. Control blanks were also prepared using 1 mL of buffer. Five 1:1 serial dilutions with buffer were made in sterile culture tubes to create a range of peptide concentrations. The final volume in all the tubes was either 300 μL or 1 mL. Agar medium (2.7 or 4.5 mL) was added to each tube, and the contents were mixed. Aliquots (1 mL) of each were added to a 24-well plate to give six different concentrations of each peptide per plate. Each plate had a row of control blanks and a row of a positive control. A stock ketoconazole solution (10 mg/mL in DMSO) was diluted 1:49 with buffer. A range of final concentrations from 20 to 0.63 μg/mL was tested which encompasses the known minimum inhibitory concentration of ketoconazole (1.25 μg/mL) against *S. cerevisiae* (*31*). Hst5 or Hst3 was tested in a

range from 200 to 6.3 μM. Cyclic analogues were tested at concentrations ranging from 200 to 0.14 μM until the analogue with the lowest MIC was identified. An isolated colony of *S. cerevisiae* was picked from an SDA plate aseptically and cultured overnight in growth media (5 mL) at 30 °C, with shaking at 125 rpm. Cells grown overnight were centrifuged and washed with a 0.85% saline solution (three times). The cell concentration was adjusted to 85% transmission at a λ of 530 nm with saline solution. Cells were further diluted 1:19 with saline. Inoculant (10 μL) was added to the surface of each well on the plate. The cells were incubated on this medium for 16−36 h at 37 °C. The fungistatic MIC for these compounds was defined as the minimum concentration required to achieve 100% growth inhibition after visible growth in the control wells.

CD Spectroscopy

Sample Preparation. Peptide concentrations were calculated from the UV absorbance of tyrosine residues at a wavelength of 275 nm [$\epsilon = 1390$ (*33*)]. A range of peptide concentrations was analyzed initially to establish that mean residue ellipticity was essentially independent of peptide concentration, and then the peptide concentration that gave the best signal-to-noise ratio was used in subsequent measurements. CD samples were prepared with a final peptide 4 concentration of 20 μM and a final Hst3 concentration of 100 μM in 5 mM potassium phosphate buffer at pH 7.2 with varying concentrations of distilled trifluoroethanol (TFE) or L-α-dimyristoylphosphatidylcholine (L-α-DMPC). Small unilamellar L-α-DMPC vesicles were prepared following the method of Signor and co-workers (*34*). The lipid was dissolved in spectroscopic grade $CHCl_3$ (22 mg in 5 mL). This solution was evaporated to dryness using a rotary evaporator. The dry lipid was redissolved in Milli-Q water (5 mL) and sonicated until the turbidity at 400 nm had cleared to a constant minimum absorbance (~1.5 h). The peptide was then added to the solution to create various lipid-to-peptide ratios. The bigger liposomes were then removed using a 0.45 μm filter to improve the signal-to-noise ratio (*35*).

CD Measurements. CD measurements were taken using a rectangular quartz cell with a path length of 0.1 cm. The temperature was maintained at 25 °C with a Peltier temperature control unit. The L-α-DMPC samples were run at 30 °C so that they would be above the phase transition temperature for these lipids. Measurements were taken over a range of 250−190 nm, a scan speed of 100 nm/min with a sensitivity of 50 mdeg, a resolution of 0.5 nm, and a bandwidth of 1.0 nm. Typically, eight scans were accumulated and averaged. The CD spectrum of the buffer or lipid solution was subtracted from all dichroic spectra, which were then smoothed. The CD spectra are reported as the mean residue molar ellipticity ([θ]) in degrees per square centimeter per decimole.

NMR Spectroscopy

Sample Preparation. Samples for NMR spectroscopy were prepared as ~5 mM solutions of lyophilized peptide in 10 mM potassium phosphate buffer. The pH was adjusted to 7.3 with ammonium hydroxide prior to the NMR experiments. To obtain the lock signal, 10% D_2O was added, and the final volume was 500 μL. Sodium 3-(trimethylsilyl)-2,2,3,3-d_4 propionate (TSP) was used as an internal chemical shift reference. Samples containing L-α-DMPC-d_{54} were prepared as in the CD experiments at a final concentration of 50 mM to give a lipid-to-peptide ratio of 10:1. The pH of the peptide solution with L-α-DMPC-d_{54} was determined to be 7.6. The NMR experiments were carried out at 300 K for aqueous samples and 303 K for samples containing L-α-DMPC-d_{54}. The pH titration samples were prepared in a manner similar to that of the aqueous samples and adjusted to 10 pH values between 3.3 and 9.6. Solutions were adjusted to the desired pH with 0.1 M HCl or 0.1 M NaOH. The pH values of NMR solutions were determined by direct pH-meter reading without correction for deuterium isotope effects.

NMR Procedures. All NMR measurements were recorded at a ^{1}H frequency of 500 MHz on a Bruker AMX-500 NMR spectrometer. A Bruker BVT-2000 temperature control unit was used to maintain temperatures. The spectrometer was equipped with either an inverse triple-resonance probe with actively shielded *z*-gradients or with an inverse broadband probe. Two-dimensional homonuclear ^{1}H NMR spectra were acquired in the phase-sensitive mode using the States method (*36*). Water suppression was achieved by either a 1.5 s selective low-power irradiation of the water signal or the 3-9-19-19-9-3 WATERGATE sequence prior to acquisition (*37*). The two-dimensional (2D) NMR data for all Hst3 experiments and for peptide 4 in the presence of L-α-DMPC-d_{54} were acquired with 16 scans per increment for 1024 T_1 increments while collecting 4096 complex data points. Resolution enhancement of the time domain data was achieved by applying a $\pi/2$ phase-shifted squared sine-bell function in both dimensions. A final matrix of 4096 × 2048 points was obtained after zero-filling. The 2D data were collected in the following manner for the aqueous sample of peptide 4. Each of 512 T_1 increments was acquired with 64 scans of 2048 complex data points and a spectral width of 5378 Hz in both dimensions. During processing, the raw data were zero-filled to produce transformed matrixes of 2048 × 1024 points, and both dimensions were multiplied by a $\pi/2$ phase-shifted squared sine-bell function.

All NOESY experiments for Hst3 were carried out with the application of a pulsed field gradient during the mixing time (*38*). To suppress zero quantum coherence, the mixing time was varied up to 5% of its value for each increment (*39*). Peptide 4 NOESY experiments were carried out using standard methods (*40*). NOESY experiments performed for the purpose of conformational analysis were repeated with various mixing times between 50 and 600 ms. TOCSY experiments (*41*, *42*) employed the MLEV-17 pulse sequence to obtain a 100 ms spin lock at a field strength of approximately 9 kHz.

TOCSY experiments for the pH titration were carried out using four scans per increment for 128 T_1 increments collecting 1024 complex points. The spin lock time for these experiments was 100 ms. The processing of these spectra was carried out as described above except that the raw data were zero-filled to 1024 × 512 transformed matrices. From previous sequential assignments of Hst3 (*24*) and of peptide 4 in aqueous solution at high and low pH, the chemical shifts of the histidine ring protons of both peptides were recorded as a function of pH. These values were then imported into

Microcal Origin for nonlinear least-squares fitting to the following equation:

$$\delta(\mathrm{pH}) = \frac{\delta_b + \delta_a \times 10^{\mathrm{p}K_a - \mathrm{pH}}}{1 + 10^{\mathrm{p}K_a - \mathrm{pH}}}$$

where δ(pH) is the measured chemical shift of the histidine ring proton at the given pH (parts per million), δ_b is the limiting chemical shift at high pH (parts per million), and δ_a is the limiting chemical shift at low pH (parts per million).

This equation is derived from the Henderson−Hasselbach equation for the ideal curve of a resonance with a single apparent ionization constant, pK_a (*43*).

The strengths of ^{1}H−^{1}H NOEs were determined from NOE cross-peak intensities in the NOESY spectra. The βH−βH cross-peaks of F^{14}, Y^{28}, Y^{30}, and/or D^{31} for Hst3 and Y^5 and/or Y^{19} for peptide 4 were selected as references (1.74 Å), depending on overlap, to calibrate the intensities against known distances (*44*). The relative intensities of the cross-peaks were then classified as strong, medium, or weak corresponding to upper bounds of 2.5, 3.5, and 6.0 Å, respectively, depending on their intensity (*44*).

A preliminary model of the conformation of peptide 4 in aqueous solution was made by incorporating the 21 long-range NOE restraints found for this peptide. The ^{1}H−^{1}H distances for structure determination were deduced from NOE cross-peak intensities in the 100 ms NOESY spectrum. The cross-peaks were assigned distance range restraints of 1.8−6.0, 1.8−3.5, and 1.8−2.5 Å based on the volumes of cross-peaks integrated by the NMR analysis program Felix (*44*). A total of 108 NOE distance range restraints were added to the random structure of cyclized peptide 4. This structure was subjected to restrained energy minimization using the Sybyl 6.3 molecular modeling package. This restrained energy minimization consisted of 1000 iterations with the application of conjugate gradients (*45*), employing the Kollman-all-atom force field and Kollman charges (*46*) and a dielectric constant of 1 until the rms gradient was smaller than 0.05 kcal mol^{-1} Å^{-2}. The minimization was repeated until there were no distance violations greater than 0.3 Å. The structure was then evaluated for torsional strain and adjusted until only four torsional angles were not satisfied.

RESULTS

Conformational Analysis of Hst3. The CD spectra of Hst3 in the presence of small unilamellar vesicles of L-α-DMPC are shown in Figure 1. In this case, there is a dramatic decrease in the minimum at 198 nm in the CD spectra upon addition of L-α-DMPC; however, no typical pattern for a regular secondary structure is observed.

From the NOESY spectra recorded between 50 and 600 ms for each peptide, the NOE cross-peak intensities were evaluated as a function of mixing time. They were found to be linear for mixing times of up to 300 ms for Hst3 (data not shown). Histatins contain several identical amino acids that complicate the sequential assignment, particularly for Hst3. However, all repeated residues were assigned through connectivities to β-protons and adjacent residues.

Figure 2 illustrates the proton connectivities observed for Hst3 in L-α-DMPC lipid vesicles. Of particular note in both cases are the strong N−N(i, i + 1) NOEs at the C-terminus

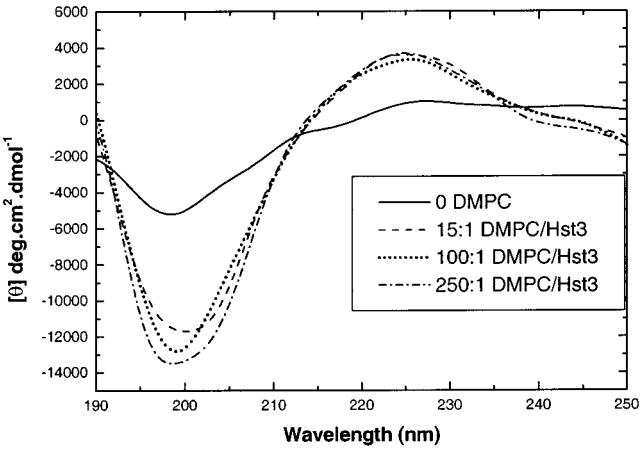

FIGURE 1: CD spectra of Hst3 in aqueous solution with increasing concentrations of L-α-DMPC small unilamellar vesicles.

and the strong long-range interactions between residues Y^{10} and S^{20} as well as the weak interaction between Y^{10} and N^{27} listed in other NOE data in Figure 2. This is suggestive of a structured C-terminus and interactions between regions near residues 10 and 20.

The pH titration of Hst3 in aqueous solution was carried out over a pH range of 3.3−9.5. The peptide precipitated at pH values above 9.5. There were three groups of chemical shifts representing the ring protons of (a) H^3, H^7, H^{18}, and H^{21}, (b) H^8 and H^{19}, and (c) H^{15}. These groupings were verified by earlier sequential assignments made at pH 3.8 and 8.5. The pK_a values for these three groups of histidines are listed in Table 1.

The pK_a values from both ring protons of each histidine group were in agreement to approximately ±0.30 and range from 6.55 to 7.02. These pK_a values are below the pH of the NMR experiments performed with L-α-DMPC.

Antifungal Activity. The MIC values for the cyclic analogues are summarized in Table 2. Initially, analogues were tested in the same range as Hst5. Once analogues were determined to be more active than Hst5, the testing range was lowered to that of the most active peptide. Peptides whose MIC was higher than the current range were not retested to give an exact MIC value. The MIC of ketoconazole, which was found to be 1.25−2.5 μg/mL, compared favorably with the literature value of 1.25 μg/mL for activity against *S. cerevisiae* (*31*). Peptide 4 was found to be the most active against *S. cerevisiae* (0.30−0.60 μM), being approximately 100 times more potent than Hst5 and 8 times more potent than ketoconazole. The linear form of peptide 4 was found to have an MIC of >5.0 μM.

CD Spectroscopy. The CD spectrum of peptide 4 in buffer solution reveals only a positive band at 225 nm. CD spectral analysis of peptide 4 was performed with different concentrations of TFE and with increasing concentrations of small unilamellar vesicles of L-α-DMPC. The magnitude of the positive band at 225 nm diminishes with increasing concentrations of TFE, while a minimum at 208 nm and a positive band at 195−200 nm appear (Figure 3). Only at a 200:1 L-α-DMPC lipid-to-peptide ratio is there a significant change in the CD spectrum with a slight minimum at 205−215 nm and a positive peak at 200 nm appearing (Figure 4). This is unlike Hst3 which exhibited a significant change in the CD spectrum even upon addition of a 15-fold excess of L-α-

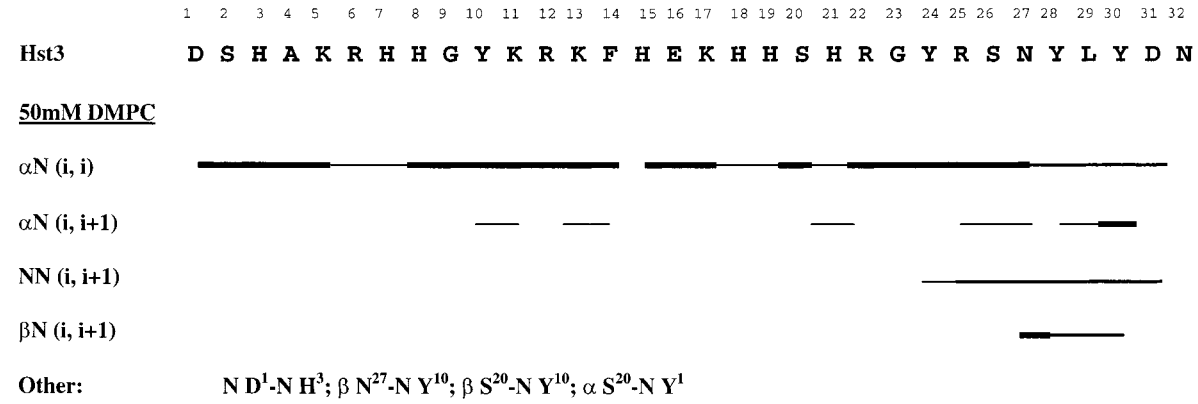

FIGURE 2: Summary of sequential and medium-range NOE data obtained from the NOESY spectra of Hst3 recorded with a mixing time of 300 ms. Strong (thick lines), medium (medium lines), and weak (thin lines) NOEs are indicated. Again only significant NOEs were depicted in this figure. Interesting longer-range NOEs that are of no particular pattern are listed under the category other.

Table 1: pK_a Values for Histidine Residues of Hst3 in 10 mM Phosphate Buffer at 298 K[a]

histidine	C4 pK_a	C2 pK_a	average pK_a
3, 7, 18, 21	6.42 ± 0.14	6.67 ± 0.12	6.55 ± 0.26
8, 19	6.89 ± 0.19	6.70 ± 0.12	6.79 ± 0.31
15	6.98 ± 0.17	7.06 ± 0.09	7.02 ± 0.26

[a] Error estimates were obtained from the nonlinear least-squares fitting program.

Table 2: Fungistatic Activity of Hst5 and Cyclic Histatin Analogues against *S. cerevisiae*

Code	Peptide Sequence	MIC Range (μM)
Hst3	DSHAKRHHGYKRKFHEKHHSHRGYRSNYLYDN	25.0-50.0
Hst5	DSHAKRHHGYKRKFHEKHHSHRGY	25.0-50.0
Peptide 1[a]	DSHAKRHHCYKRKFHEKHHSHRCY	20.0-40.0
Peptide 2[a]	RHHCYKRKFHEKHHSHCGY	6.25-12.5
Peptide 3[a]	RHHCYKRKFHEKHHSCRGY	0.63-1.26
Peptide 4[a]	RHHCYKRKFHEKHHCHRGY	0.30-0.60
Peptide 5[a]	RHHCYKRKFHEKHCSHRGY	2.50-5.00
Peptide 6[a]	RHHGCKRKFHEKHHSHCGY	0.63-1.25
Peptide 7[b]	RHHKYKRKFHEKHHEHRGY	0.55-1.10
	Ketoconazole	2.35-4.70

[a] This peptide is cyclized via disulfide bond formation. [b] This peptide is cyclized via an amide bond between side chains.

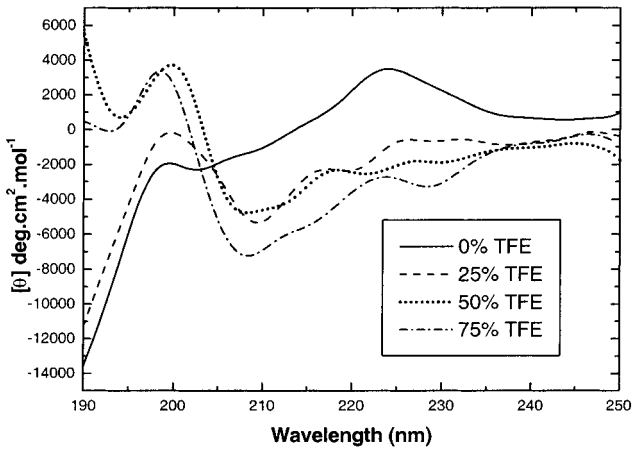

FIGURE 3: CD spectra of peptide 4 in H_2O with increasing concentrations of TFE.

DMPC lipid (Figure 1). The conformation of peptide 4 undergoes only modest conformational change in either environment that was examined, indicating its stability.

NMR Spectroscopy. Sequential assignment of peptide 4 was made from analysis of the TOCSY spectrum and the

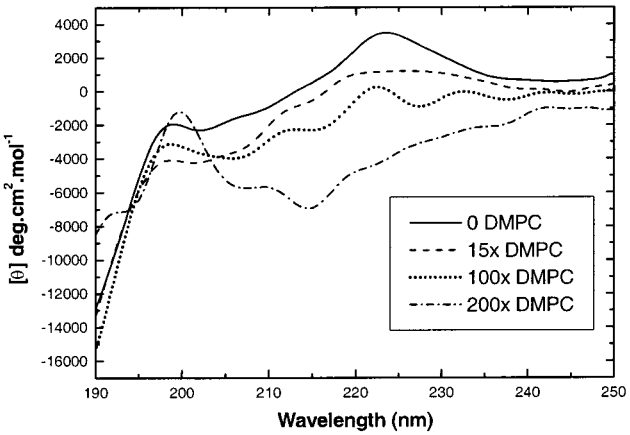

FIGURE 4: CD spectra of peptide 4 in aqueous solution with increasing concentrations of L-α-DMPC small unilamellar vesicles.

Table 3: Proton Chemical Shifts of Peptide 4 in Phosphate Buffer (pH 7.3) at 300 K

residue	NH	CαH	Cβ H	others
Arg6			1.75	Cγ H 1.53, Cδ H 3.11
His7	8.42	4.50	2.96, 3.05	4H 6.85, 2H 7.64
His8	8.45	4.56	2.95, 3.04	4H 6.85, 2H 7.74
Cys9	8.35	4.45	3.82, 3.94	
Tyr10	7.52	4.40	2.91, 3.08	3,5H 7.04, 2,6H 6.78
Lys11	8.36	4.21	1.73	Cγ H 1.33, Cδ H 1.63, Cϵ H 2.96
Arg12	8.19	4.25	1.62, 1.78	Cγ H 1.44, Cδ H 3.05
Lys13	8.43	4.21	1.74	Cγ H 1.35, Cδ H 1.63, Cϵ H 2.94
Phe14	7.63	4.38	2.87, 3.05	2,6H 7.17, 3,5H 7.47, 4H 7.34
His15	8.31	4.56	2.94, 3.07	4H 6.96, 2H 7.78
Glu16	8.19	4.21	1.92, 2.03	Cγ H 2.17
Lys17	8.27	4.21	1.78	Cγ H 1.28, Cδ H 1.62, Cϵ H 2.93
His18	8.18	4.52	2.96, 3.10	4H 6.93, 2H 7.67
His19	8.37	4.58	2.95, 3.08	4H 6.96, 2H 7.70
Cys20	8.35	4.45	3.79, 3.95	
His21	8.27	4.47	2.93, 3.07	4H 6.93, 2H 7.67
Arg22	8.17	4.30	1.67, 1.80	Cγ H 1.57, Cδ H 3.10
Gly23	7.49	3.94		
Tyr24	7.71	4.39	2.86, 3.06	3,5H 6.81, 2,6H 7.11

50 and 100 ms NOESY spectra. This shorter constrained peptide required short mixing times for us to be able to linearly correlate observed NOE intensity in the NOESY spectrum to distance. The majority of the sequential NOEs were observed in both the 50 and 100 ms NOESY spectra. The complete sequential assignment of peptide 4 in aqueous solution can be found in Table 3. Figure 5 summarizes the proton connectivities observed for the peptide in both

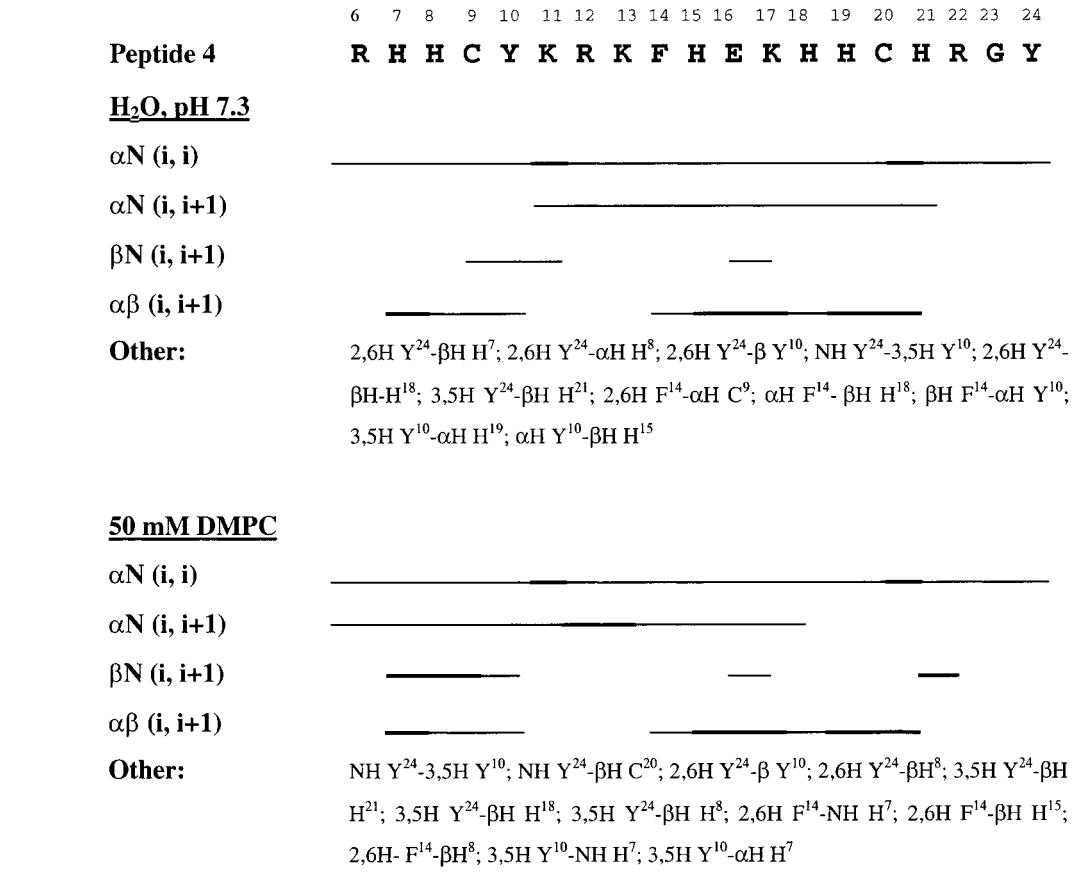

FIGURE 5: Summary of sequential and medium-range NOE data obtained from the NOESY spectra of peptide 4. Strong (thick lines), medium (medium lines), and weak (thin lines) NOEs are indicated. Only significant NOEs are listed. Interesting longer-range NOEs between aromatic residues are listed under the category other.

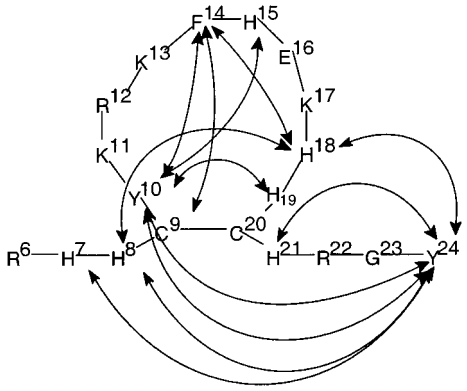

FIGURE 6: Some of the more interesting medium- and long-range ^{1}H−^{1}H NOEs between aromatic/hydrophobic residues and histidines that were found in the NOESY spectrum of peptide 4 in phosphate buffer (pH 7.3) at 300 K.

environments. Due to the small numbers of αN(i, i + 1) and βN(i, i + 1) NOEs, some of the sequential assignment was based on cross-peaks between protons further along the side chains of adjacent amino acids. The more interesting longer-range interactions between residues are shown in Figure 6. Of these long-range interactions one is strong, eight are medium, and 12 are weak NOEs.

The pH titration of peptide 4 in aqueous solution was carried out over a pH range of 3.4−9.6. The peptide precipitated at pH >9.6. All six histidine residues had distinctive ring proton chemical shifts at pH 7.3. The pK_a values for the H^2 and H^4 (C4) protons of all histidines as well as the average pK_a values for each histidine are listed in Table 4. The pK_a values for both protons of a given histidine range from 4.53 to 5.91 and were in agreement to within approximately ±0.5.

Table 4: pK_a Values for Histidine Residues of Peptide 4 in 10 mM Phosphate Buffer at 300 K[a]

histidine	C4 pK_a	C2 pK_a	average pK_a
7	5.86 ± 0.35	5.49 ± 0.17	5.68 ± 0.52
8	5.94 ± 0.25	5.70 ± 0.21	5.82 ± 0.46
15	5.01 ± 0.18	4.99 ± 0.13	5.00 ± 0.31
18	4.28 ± 0.17	4.77 ± 0.11	4.53 ± 0.28
19	6.19 ± 0.28	5.64 ± 0.19	5.91 ± 0.47
21	5.86 ± 0.24	5.62 ± 0.21	5.74 ± 0.45

[a] Error estimates were obtained from the nonlinear least-squares fitting program.

DISCUSSION

Conformational Analysis of Hst3. Most antimicrobial peptides are believed to interact strongly with biological membranes (*11*). This membrane environment may produce a conformational change in a peptide that allows its interaction with fungal cells, causing cell death either by membrane leakage or by interaction with an internal target. The use of native membranes for solution NMR studies is hampered by their slow tumbling on the NMR time scale which leads to extreme line broadening (*11*). L-α-DMPC lipid vesicles can be used to mimic the environment of a biological membrane and in some cases have been shown to induce secondary structure upon interaction with peptides (*47*). L-α-DMPC has a zwitterionic headgroup similar to those of the

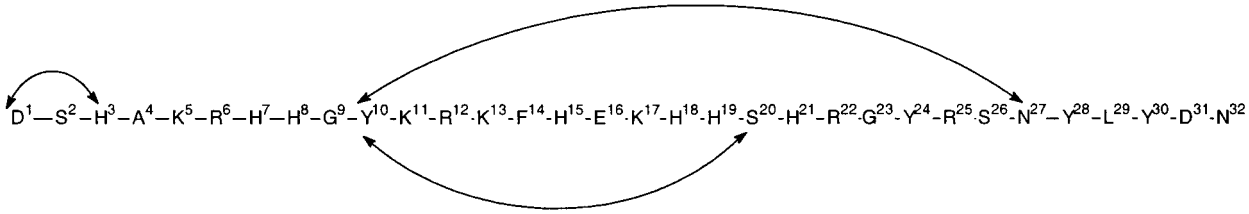

FIGURE 7: Summary of longer-range $^1H-^1H$ NOEs found in the NOESY spectra of Hst3 in the presence of L-α-DMPC lipid vesicles.

lipids that make up the majority of eukaryotic membranes. The conformation of Hst3 in L-α-DMPC was examined to assess its possible interaction with fungal membrane.

In the CD spectra of Hst3 at higher L-α-DMPC concentrations, a maximum appears at 225 nm and the magnitude of the minimum at 198 nm increases dramatically even at low lipid-to-peptide ratios (Figure 1). The presence of an isodichroic point at 210 nm suggests an equilibrium shift from a disordered to a more ordered state (*48*). The lipid vesicles do not appear to stabilize helical or β-sheet structure. This is confirmed by the NMR data where there is a lack of NOEs typical of regular secondary structure. A change in conformation is, however, supported by the NMR data which show a loss of NN(i, $i + 1$) NOEs except at the C-terminus and a weakening of the αN(i, $i + 1$) NOEs compared to Hst3 in aqueous solution (*24*). In addition, a more compact structure is suggested by the appearance of the α/βN(i, $i - 10$) S^{20}–Y^{10} NOE and the βN(i, $i - 17$) N^{27}–Y^{10} NOE (Figure 2). The observation of fewer, weaker NOEs in the region of residues 10−20 and the lack of more longer-range connectivities within the sequence suggest the presence of an open loop. The NH chemical shifts of Hst3 in the presence of L-α-DMPC are similar to those in water with the exception of an upfield shift in the region of K^{13}-Y^{24} which along with a slight line broadening indicates the interaction of Hst3 with L-α-DMPC (*49*).

The chemical shifts of histidine ring protons are averages based on the populations of the protonated and unprotonated forms that are usually in fast exchange (*50*). These values were approximately 6.55 for H^3, H^7, H^{18}, and H^{21}, 6.79 for H^8 and H^{19}, and 7.02 for H^{15} (Table 1). The pK_a values of histidine residues in proteins can range from 4.5 to 8.5 and are influenced by solvent-exposure, interacting ionizable groups, and conformation (*50*). Solvent-exposed histidines in proteins have pK_a values around 6.6 (*51*).

Two reports have found that fluorescent Hst3 and Hst5 are internalized upon interaction with *C. albicans* cells. In one study, the target for Hst5 was determined to be the mitochondrial membrane (*13*). Hst3 was found to first bind to a discrete area of the cell membrane and then to concentrate around the cell periphery before accumulating within the cells (*17*). Neither study clarified the interaction of the peptides with fungal membranes. The structural studies outlined here show some conformational change upon the interaction of Hst3 with membrane vesicles, which may play a role in the insertion and/or translocation of this peptide across the membrane. It is also possible that the fold present in Hst3 favors optimal interaction with a specific membrane lipid or protein. It has been shown previously that the translocation of Hst5 results in membrane perturbations (*53*). Other studies have shown that basic peptides are capable of being translocated across membranes and internalized into cells without the help of permeases (*54*−*56*). The structural data on Hst3 also indicate this peptide remains flexible. Flexibility in peptide structure has been suggested to be essential for peptide activity at interfaces (*48*).

From the conformational data, the structure of Hst3 appears to be relatively open in aqueous solution and adopts a more compact atypical secondary structure in membrane-like environments while remaining quite dynamic. Other peptides of similar length have also been shown to exist in multiple conformations by solution NMR (*57*−*59*). However, Hst3 in the presence of L-α-DMPC lipid vesicles was found to form a more compact structure containing a loop with residues Y^{10} and S^{20} close to each other as evidenced by long-range NOEs (Figure 7). The pK_a values for histidine residues of Hst3 in aqueous solution were all found to be below neutral pH, indicating the potential for the histidines to be in the neutral form under biologically relevant conditions. In the neutral form, histidines possess pseudoaromatic and hydrophobic character that may be significant for the folding of this peptide into its active form.

Design of Hst3 Analogues. To assess the biological relevance of this extended loop structure, cyclic analogues were designed to bring residues 10 and 20 close to each other. The antifungal activity of the analogues was subsequently tested. The purported loop was stabilized by replacing two amino acids with cysteines followed by cyclization via a disulfide bond. Initially, it was thought that the least disruptive cysteine substitutions in the histatin sequence would be at Gly^9 and Gly^{23}. The two glycines are a reasonable distance apart to contain a loop around residues 16 and 17 where a break in structure has previously been suggested (*24*). This positioning would also bring residues 10 and 20 close to each other. Optimal placement of the cysteine residues was then determined by moving one cysteine by one position at either end while keeping the other cysteine constant. Peptide 4 ($Gly^9 \rightarrow$ Cys, $Ser^{20} \rightarrow$ Cys) was found to be the most potent analogue with an MIC of 0.3 μM, which is approximately 100 times more potent than Hst5 and 8 times more potent than ketoconazole in the fungistatic assay (Table 2). This peptide is 19 amino acids long and has a loop size of 12 residues with cysteines replacing a glycine and a serine. Additional deletions at the C-terminus resulted in a slight loss of activity. The linear form of peptide 4 was also tested and found not to be active below 5.0 μM. Other cyclic peptides such as the protegrins and tachyplesins also lose both structure and activity when in the linear form (*60*, *61*). Of all other histatin-based analogues in the literature, the most improved antifungal activities were seen for the analogues of Hst3 or Hst5 where the so-called functional domain was internally repeated. The improvement varied from 1.8 times for an analogue of Hst3 (*62*) to 6 times for an analogue of Hst5 (*53*). In these cases, the analogue is

significantly longer and therefore not nearly as efficient as peptide 4.

Effecting cyclization with an amide bond between the side chains of a glutamic acid and a lysine residue (peptide 7) placed at the same positions as the cysteines in peptide 4 resulted in a peptide with activity similar to that of peptide 4 (Table 2). This confirms that the overall structure of the peptide is the determining factor in the improved activity and not the presence of the disulfide bond or of sulfur itself. The linear form of peptide 4 did not have activity in the same range ($>0.5\ \mu$M), signifying that the cyclization of the peptide is crucial for the improved activity. A peptide with the same amino acid composition as peptide 4 but in a randomized sequence was made to determine whether the sequence of amino acids is important for activity. This peptide was inactive in the concentration range that was tested ($0.33-5.35\ \mu$M), indicating that the histatin-based sequence is also crucial for optimal activity. From the analogues that were tested, it is noteworthy that the most active analogue was the one in which the cysteines did not replace a positive charge. Overall, positive charge is believed to play a critical role in the bioactivity of a number of antimicrobial peptides (*63*).

Conformational Analysis of Peptide 4. To gain further insight into the bioactive conformation of Hst3 and Hst5, conformational analysis of the most active analogue, peptide 4, was subsequently performed by CD and NMR. CD analysis of peptide 4 in buffer shows no strong minimum at 200 nm, which suggests an unordered structure (Figure 3) (*64*). There is a strong positive band at 225 nm that can be attributed to a β-turn structure (*65*). Bactenecin, which has a loop similar in size to that of peptide 4, was found to exist as a type I β-turn in aqueous solution as evidenced by the negative ellipticity at ~205 nm in the CD spectrum (*66*). With increasing concentrations of TFE, the magnitude of the positive band at 225 nm decreased while a minimum at 208 nm and a positive band at 195−200 nm appeared in the CD spectrum (Figure 3). This band at 208 nm is characteristic of a β-sheet as determined by Greenfield and Fasman (*67*). In addition to its well-known ability to stabilize helices, TFE has been shown to induce β-sheet structures in peptide fragments of similar size (*68*, *69*). In the presence of L-α-DMPC vesicles, the CD spectra of peptide 4 exhibit negligible change at 15:1 and 100:1 lipid-to-peptide ratios except for a slight decrease in the magnitude of the positive band at 225 nm (Figure 4). With a 200-fold greater concentration of lipid than peptide, a trough between 205 and 215 nm and a positive peak at 200 nm can be seen, indicative of a β-sheet. Peptide 4 is unlike brevinin 1E and ranalexin which become α-helical in membrane mimetic environments (*49*, *70*). The CD of peptide 4 has similarities to that of tachyplesin, however, which is known by NMR to contain a β-sheet connected by a β-turn and two disulfide bonds (*71*). Tachyplesin is more rigid than peptide 4, maintaining a β-sheet CD spectrum in H_2O, TFE, and liposomes, although the peak ratios change dramatically in different environments, suggesting interaction of the peptide with solvent (*64*). Even small amounts of TFE cause a conformational change in the structure of peptide 4, while large amounts of L-α-DMPC are required to induce any structural change. The structure of peptide 4 in aqueous buffer alone is unclear by CD but does appear to have some contribution from a β-turn.

The NMR data of peptide 4 in aqueous buffer have a number of interesting features and implications, the first of which is the dramatic upfield shift of the NH chemical shifts of the three aromatic residues, the six histidine residues, and the single glycine residue with respect to their chemical shifts in native histatin peptides (*24*). For example, Gly^{23} of Hst3 and Hst5 had NH chemicals shift of 8.52 and 8.42 ppm, respectively, while in peptide 4, the corresponding Gly has a chemical shift of 7.49 ppm. This corresponds to an upfield shift of approximately 1 ppm from that of the corresponding amino acids in Hst3 and Hst5 (*24*), reflecting the shielding of these NH protons. This is also indicative of a significant rearrangement of the backbone near Gly^{23}. The chemical shifts of all the histidine ring protons were found to be markedly upfield at pH 7.3 when compared to other histatin peptides under similar conditions (*24*), implying that these protons are also shielded. On the other hand, the NH chemical shifts of K^{11}, R^{12}, K^{13}, and K^{17} are downfield shifted from or equivalent to those of the corresponding residues of the parent Hst3 and Hst5.

In the NOESY spectrum of peptide 4 at pH 7.3, NN(i, $i+1$) NOEs are not detected and there are no $i-i+3/4$ cross-peaks which would indicate helical structure (Figure 5). This agrees with the CD data. In addition, there are fewer of the $i-i+1$ interactions normally observed for polypeptides, and those that are present are weaker than in Hst3 and Hst5 (*24*). There are, however, a number of weak $\alpha\beta(i, i+1)$ interactions that are visible and allow the sequential assignment to be completed. The most striking feature of the NOE data is the large number of long-range NOEs, particularly between the ring protons of the three aromatic residues to αH and βH protons of histidine residues, namely, $Y^{24}-H^{7}$, $Y^{24}-H^{8}$, $Y^{24}-H^{18}$, $F^{14}-H^{18}$, $Y^{10}-H^{19}$, and $Y^{10}-H^{15}$ (Figure 6). Some of these protons belong to residues far apart in the sequence. For instance, the NOEs between the residues at the C-terminus (Y^{24}) and near the N-terminus (H^{7} and H^{8}) indicate that the N- and C-terminal residues are close to each other. From the pH titration data, the C2 proton signals of histidine residues shift upfield by an average of almost 1 ppm and the C4 proton signals shift by ~0.4 ppm on average. This is consistent with deprotonation of this side chain (*50*). All the pK_a values are lower than would be expected for a histidine residue exposed to solvent (Table 4) (*72*). The lowest pK_a values are for H^{15} and H^{18}, which are in the middle of the loop. These data strongly suggest that the three aromatic residues and some or all of the histidine residues cluster in the inner core while the charged amino acid side chains are separated and on the outer surface. This hypothesis was corroborated by the energy minimization of NOE distance restraints into the random structure of the disulfide-bonded peptide 4. Figures 8 and 9 illustrate the proposed conformation of peptide 4 in aqueous solution calculated from the energy minimization of NOE distance restraints that were found for this peptide in aqueous solution by NMR.

The N- and C-termini are folded to interact with residues within the loop to produce the long-range NOEs observed in the NMR data (Figure 8). The structure in Figures 8 and 9 depicts the aromatic core and the hydrophilic external surface of peptide 4. The cluster of aromatic rings in the inner core accounts for the upfield shift of the NH protons

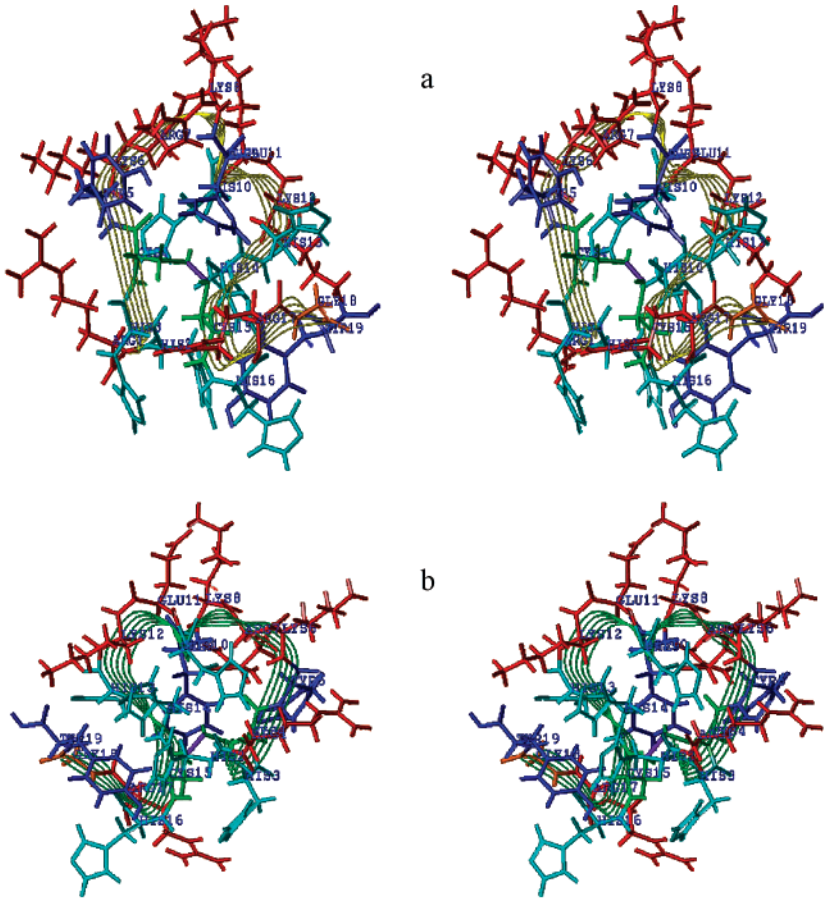

FIGURE 8: Stereoview of the proposed structure of peptide 4 in aqueous solution deduced from NMR data: (a) front view and (b) back view. Charged residues are in red. Aromatic residues are in blue. Histidines are in cyan. Glycine is in orange. Cysteines are in green. Residues are numbered chronologically.

of these residues. The tight turn at the top of the loop and the interactions across the face of the loop correlate with the CD data that suggest a β-sheet with a β-turn. This turn at the top of the loop is likely a result of the electrostatic interactions among K^{13}, E^{16}, and K^{17}. The NMR analysis of the full-length Hst3 indicated the presence of a turn centered in the region of residues $K^{11}-K^{17}$ (*24*). The pH titration data correlate well with these models, showing pK_a values that could indicate that some or all of the histidines are in the neutral form and thus taking part in a hydrophobic core. The particularly low pK_a values for H^{15} and H^{18} and their location in the model structure suggest they are unprotonated and most likely buried. In proteins, lower pK_a values are typically seen for residues buried in structural elements or in a hydrophobic core (*51*, *73*).

The structure of peptide 4 was also examined in membrane-mimicking environments to determine the stability of this compact peptide when in the presence of lipid model systems. The NMR analysis of peptide 4 in the presence of L-α-DMPC vesicles shows an upfield shift for the same NH chemical shifts as was found in the aqueous sample when compared to the values of Hst3. There are only two significant changes in NH chemical shifts compared to the aqueous sample of peptide 4. H^8 is upfield shifted in lipid, while H^{19} is downfield shifted. The pattern of NOEs observed under these conditions for the inter-residue or sequential proton interactions is similar to that of peptide 4 in buffer (Figure 5). There is an increase in the number of long-range NOEs, which again primarily occur between the ring protons of the aromatic residues and the αH, βH, and even NH protons of the histidines. Thus, the structure of peptide 4 in a membrane mimetic environment is very similar to that in buffer but appears to be even more compact.

The proton−proton interactions within peptide 4 remain relatively constant in different environments. On the other hand, the interactions within Hst3 change between the two environments that were examined. This is indicative of the rigidity of peptide 4 with only a single disulfide bond versus the flexibility of the linear Hst3. Overall, the calculated structure of peptide 4 in aqueous solution is energetically favorable as it allows the positively charged amino acids to be as far apart as possible and to interact with solvent while creating a hydrophobic core composed of the three aromatic residues and at least four histidines.

Implications for Activity. The sequence of peptide 4 does not have the typical amphipathic character found in most other antimicrobial peptides. The structure deduced from NMR analysis, however, shows a definite hydrophilic external surface with a nonpolar core that includes some or all of the histidine residues. From the pH titration data, it is clear that at least H^{15} and H^{18} are uncharged at neutral pH. This would allow aromatic stacking of these side chains with F^{14}, Y^{10}, and Y^{24}. The spatial proximity of aromatic residues within an amino acid sequence has been observed in small peptides (*74*, *75*) and proteins (*76*).

There are some structural similarities between peptide 4 and lactoferricin B (*3*) and tachyplesin (*64*). Lactoferricin B has also been found to have a slightly distorted β-sheet

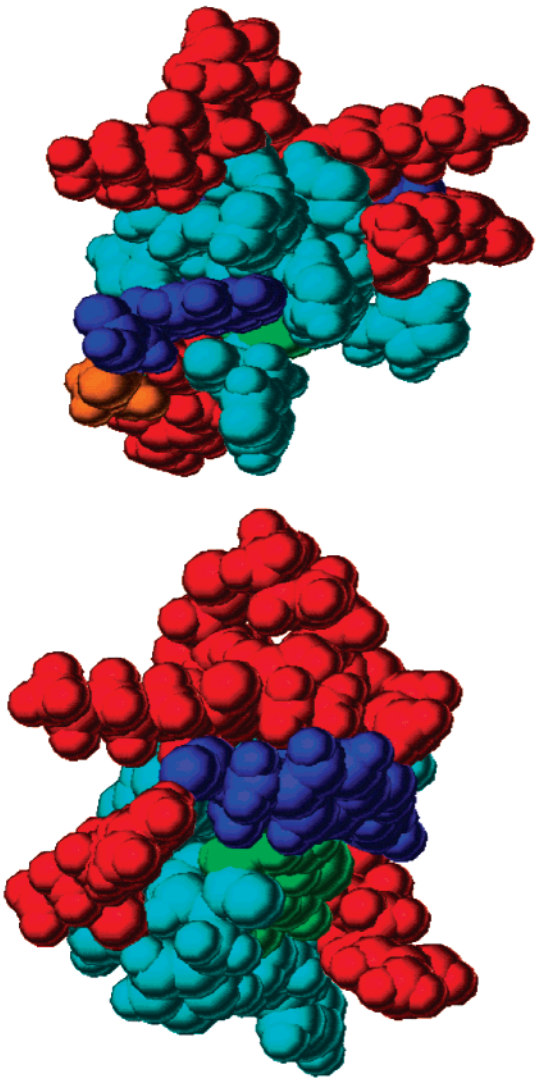

FIGURE 9: Space-filling models of the proposed structure of peptide 4 showing two faces rotated horizontally by 90°. Charged residues are in red. Aromatic residues are in blue. Histidines are in cyan. Glycine is in orange. Cysteines are in green.

structure with a hydrophobic surface made up of residues from both strands of the sheet surrounded by hydrophilic residues (*3*). In tachyplesin, the bulky hydrophobic groups are localized to the head of a rigid antiparallel β-sheet structure linked by a β-turn to a hydrophilic tail made up of cationic residues from both the N- and C-termini (*64*).

Cell localization studies have suggested that Hst3 and Hst5 mediate cell killing with an event that takes place within the cell (*12*, *52*). The first step, regardless of the presence of an internal target, requires interaction with a fungal membrane. The constrained nature of peptide 4 may position the charged residues for optimal interaction with the membrane and/or maximal interaction with the intracellular target. It also can be concluded unequivocally from the structure of peptide 4 that helicity is not an important factor for antifungal activity. Since peptide 4 incorporates the loop observed in Hst3, it is highly likely that the improvement in activity is due to the stabilization of the bioactive conformation of histatins.

Preliminary toxicity studies in mice indicated that peptide 4 is devoid of the hemolytic activity (data not shown) found with the majority of amphipathic antimicrobial peptides (*3*). This is also true for Hst5 (*13*), suggesting this sequence has low hemolytic potential. The serum half-life of peptide 4 is approximately 4 times greater than that of Hst5 (data not shown). Thus, in addition to an increase in antifungal activity, cyclization in peptide 4 markedly improved its in vivo stability. These results have prompted the filing of a patent on cyclic histatin peptides (*77*).

In summary, it was observed that Hst3 exits in multiple unstructured conformations in aqueous solution. However, it was found that Hst3 interacts with lipid vesicles and that this interaction causes a conformational change. This conformational change resulted in a more folded structure of Hst3 that contains an extended loop. It was then possible to design cyclic peptide analogues which mimic the observed loop in the middle of the sequence. Stabilization of this loop by a disulfide or a lactam bridge resulted in a remarkable enhancement in biological activity. The most active analogue against *S. cerevisiae* was peptide 4 with a 100-fold increase in activity compared to Hst5. The conformational analysis of the cyclic histatin-based analogue, peptide 4, by CD and NMR spectroscopy in aqueous solution has revealed a much more compact structure in which hydrophilic residues protrude to the external surface while aromatic residues and histidine residues cluster together in a core. These results suggest that Hst3 adopts a structure similar to that of its biological target.

ACKNOWLEDGMENT

We are very grateful to Dr. Guy Guillemette for his help with the CD measurements and the use of his CD spectrometer. We thank Dr. Randy Irvine for the preliminary toxicity and stability studies of peptide 4.

SUPPORTING INFORMATION AVAILABLE

Full proton chemical shift assignments for Hst3 in 50 mM L-α-DMPC-d_{54} at 303 K, full proton chemical shift assignments for peptide 4 in 50 mM L-α-DMPC at 303 K, and a full list of NOE distance restraints used for the modeling of peptide 4 in phosphate buffer (pH 7.3) at 300 K from the 100 ms NOESY spectrum. This material is available free of charge via the Internet at http://pubs.acs.org.

REFERENCES

1. Troxler, R. F., Offner, G. D., Xu, T., Vanderspek, J. C., and Oppenheim, F. G. (1990) *J. Dent. Res. 69*, 2−6.
2. Xu, T., Telser, E., Troxler, R. F., and Oppenheim, F. G. (1991) *Infect. Immun. 59*, 2549−2554.
3. Hwang, P. M., and Vogel, H. J. (1998) *Biochem. Cell Biol. 76*, 235−246.
4. White, T., Marr, K., and Bowden, R. (1998) *Clin. Microbiol. Rev. 11*, 382−402.
5. Oppenheim, F. G., Xu, T., McMillan, F. M., Levitz, S. M., Diamond, R. D., Offner, G. D., and Troxler, R. F. (1988) *J. Biol. Chem. 263*, 7472−7477.
6. Murakami, Y., Nagata, H., Shizukuishi, S., Nakashima, K., Okawa, T., Takigawa, M., and Tsunemitsu, A. (1994) *Biochem. Biophys. Res. Commun. 198*, 274−280.
7. Sabatini, L. M., and Azen, E. A. (1989) *Biochem. Biophys. Res. Commun. 160*, 495−502.
8. Oppenheim, F. G., Yang, Y., Diamond, R. D., Hyslop, D., Offner, G. D., and Troxler, R. F. (1986) *J. Biol. Chem. 261*, 1177−1182.
9. Taniguchi, S., Takemura, A., Matsuda, N., and Tsunemitsu, A. (1994) *Chem. Abstr. 123*, 350366.

10. Matsuda, N., Takemura, A., and Taniguchi, S. (1993) *Chem. Abstr. 122*, 89439.
11. Epand, R. M., and Vogel, H. J. (1999) *Biochim. Biophys. Acta 1462*, 11−28.
12. Edgerton, M., Koshlukova, S., Lo, T., Chrzan, B., Straubinger, R., and Raj, P. A. (1998) *J. Biol. Chem. 273*, 20438−20447.
13. Helmerhorst, E. J., Breeuwer, P., van't Hof, W., Walgreen-Wetering, E., Oomen, L. C. J. M., Veerman, E. C. I., Nieuw Amerongen, A. V., and Abee, T. (1999) *J. Biol. Chem. 274*, 7286−7291.
14. Gyurko, C., Lendenmann, U., Troxler, R. F., and Oppenheim, F. G. (2000) *Antimicrob. Agents Chemother. 44*, 348−354.
15. Koshlukova, S. E., Araujo, M. W., Baev, D., and Edgerton, M. (2000) *Infect. Immun. 68*, 6848−6856.
16. Edgerton, M., Koshlukova, S. R., Araujo, M. W. B., Patel, R. C., Dong, J., and Bruenn, J. A. (2000) *Antimicrob. Agents Chemother. 43*, 3310−3316.
17. Xu, Y., Ambudkar, I., Yamagishi, H., Swain, W., Walsh, T. J., and O'Connell, B. C. (1999) *Antimicrob. Agents Chemother. 43*, 2256−2262.
18. Raj, P. A., Soni, S.-D., and Levine, M. J. (1994) *J. Biol. Chem. 269*, 9610−9619.
19. Raj, P. A., Marcus, E., and Sukumaran, D. K. (1998) *Biopolymers 45*, 51−69.
20. Melino, S., Rufini, S., Sette, M., Morero, R., Grottesi, A., Paci, M., and Petruzzelli, R. (1999) *Biochemistry 38*, 9626−9633.
21. Raj, P. A., Edgerton, M., and Levine, M. J. (1990) *J. Biol. Chem. 265*, 3898−3905.
22. Ramalingam, K., Gururaja, T., Ramasubbu, N., and Levine, M. J. (1996) *Biochem. Biophys. Res. Commun. 225*, 47−53.
23. Helmerhorst, E. J., van't Hof, W., Breeuwer, P., Veerman, E. C. I., Abee, T., Troxler, R. F., Nieuw Amerongan, A. V., and Oppenheim, F. G. (2001) *J. Biol. Chem. 276*, 5643−5649.
24. Brewer, D., Hunter, H., and Lajoie, G. (1998) *Biochem. Cell Biol. 76*, 247−256.
25. Fields, G. B., and Noble, R. L. (1990) *Int. J. Pept. Protein Res. 35*, 161−214.
26. Wang, S.-W. (1973) *J. Am. Chem. Soc. 95*, 1328−1333.
27. Solé, N. A., and Barany, G. (1992) *J. Org. Chem. 57*, 5399−5403.
28. Andreu, D., and Rivas, L. (1999) *Biopolymers 47*, 415−433.
29. Kunz, H., and Waldmann, A. (1983) *Angew. Chem., Int. Ed. Engl. 23*, 71−72.
30. Solé, N. A., Kates, S. A., Albericio, F., and Barany, G. (1994) in *Peptides: Chemistry, Structure and Biology* (Hodges, R. S., and Smith, J. A., Eds.) pp 93−94, ESCOM, Leiden, The Netherlands.
31. Gordon, M. A., Lapa, E. W., and Passero, P. G. (1988) *J. Clin. Microbiol. 26*, 1874−1877.
32. Odds, F. C., Gordon, M. A., Lapa, E. V., and Passero, P. G. (1993) *Antimicrob. Agents Chemother. 37*, 685−691.
33. Brandts, J. F., and Kaplan, L. J. (1973) *Biochemistry 12*, 2011−2024.
34. Signor, G., Mammi, S., Peggion, E., Ringsdorf, H., and Wagenknecht, A. (1994) *Biochemistry 33*, 6659−6670.
35. Litman, J. B. (1972) *Biochemistry 11*, 3243−3247.
36. States, D., Haberkorn, R., and Ruber, D. (1982) *J. Magn. Reson. 48*, 286−292.
37. Piotto, M., Saudek, V., and Sklenar, V. (1992) *J. Biomol. NMR 2*, 661−665.
38. Wagner, R., and Berger, S. (1996) *J. Magn. Reson., Ser. A 123*, 119−121.
39. Macura, S., Huang, Y., Suter, D., and Ernst, R. R. (1981) *J. Magn. Reson. 43*, 259−262.
40. Jeener, J., Meier, B. H., Bachmann, P., and Ernst, R. R. (1979) *J. Chem. Phys. 71*, 4546−4550.
41. Bax, A., and Davis, D. G. (1985) *J. Magn. Reson. 65*, 355−360.
42. Kumar, A., Ernst, R. R., and Wüthrich, K. (1980) *Biochem. Biophys. Res. Commun. 95*, 1−6.
43. Schrager, R. I., Cohen, J. S., Heller, S. R., Sachs, D. H., and Schecther, A. N. (1972) *Biochemistry 11*, 541−547.
44. Barsukov, I., and Lian, L.-Y. (1993) in *NMR of Macromolecules: A Practical Approach* (Roberts, G., Ed.) pp 315−357, Oxford University Press, New York.
45. Powell, M. J. D. (1977) *Math. Programming 12*, 241−254.
46. Weiner, S. J., Kollman, P. A., Nguyen, D. T., and Case, D. A. (1986) *J. Comput. Chem. 7*, 230−252.
47. Rozek, A., Friedrich, C. L., and Hancock, R. E. W. (2000) *Biochemistry 39*, 15765−15774.
48. Bruch, M. D., Cajal, Y., Koh, J. T., and Jain, M. K. (1999) *J. Am. Chem. Soc. 121*, 11993−12004.
49. Vignal, E., Chavanieu, A., Roch, P., Chiche, L., Grassy, G., Calas, B., and Aumelas, A. (1998) *Eur. J. Biochem. 253*, 221−228.
50. Feeney, J., and Birdsall, B. (1993) in *NMR of Macromolecules: A Practical Approach* (Roberts, G. C. K., Ed.) pp 183−215, Oxford University Press, New York.
51. Plesniak, L. A., Connelly, G. P., Wakarchuk, W. W., and McIntosh, L. P. (1996) *Protein Sci. 5*, 2319−2328.
52. Helmerhorst, E. J., Breeuwer, P., van't Hof, W., Walgreen-Wetering, E., Oomen, L. C. J. M., Veerman, E. C. I., Nieuw Amerongen, A. V., and Abee, T. (1999) *J. Biol. Chem. 274*, 7286−7291.
53. Helmerhorst, E. J., Van't Hof, W., Veerman, E. C. I., Simoons-Smit, I., and Nieuw Amerongen, A. V. (1997) *Biochem. J. 326*, 39−47.
54. Maduke, M., and Roise, D. (1993) *Science 260*, 364−367.
55. Matsuzaki, K., Murase, O., Fijii, N., and Miyajima, K. (1995) *Biochemistry 34*, 6521−6526.
56. Matsuzaki, K., Nakamura, A., Murase, O., Sugishita, K., Fujii, N., and Miyajima, K. (1997) *Biochemistry 36*, 2104−2111.
57. Dyson, H. J., Merutka, G., Waltho, J. P., Lehrer, R. A., and Ubright, P. E. (1992) *J. Mol. Biol. 226*, 795−817.
58. Reymond, M. T., Hwo, S., Duggan, B., Ubright, P. E., and Dyson, J. H. (1997) *Biochemistry 36*, 5234−5244.
59. Yang, J. J., Bick, M., Pitkeathly, M., Kotik, M., Haynie, D. T., Dobson, C. M., and Eadford, S. E. (1995) *J. Mol. Biol. 252*, 483−491.
60. Qu, X., Harwiss, S. S., Schafer, W. M., and Lehrer, R. I. (1997) *Infect. Immun. 65*, 636−639.
61. Tamamura, H., Ikoma, R., Niwa, M., Funakoshi, S., and Fujii, N. (1993) *Chem. Pharm. Bull. 41*, 975−980.
62. Zuo, Y., Xu, T., Troxler, R. F., Li, J., and Oppenheim, F. G. (1995) *Gene 161*, 87−91.
63. Boman, H. G. (1995) *Annu. Rev. Immunol. 13*, 61−92.
64. Wu, M., and Hancock, R. E. W. (1999) *J. Biol. Chem. 274*, 29−35.
65. Rao, A. G. (1999) *Arch. Biochem. Biophys. 361*, 127−134.
66. Chang, C. T., Wu, C. S., and Yang, J. T. (1978) *Anal. Biochem. 91*, 13−17.
67. Greenfield, N., and Fasman, G. D. (1969) *Biochemistry 8*, 4108−4116.
68. Lu, Z. X., Fok, K. F., Erickson, B. W., and Hugli, T. E. (1984) *J. Biol. Chem. 259*, 7367−7370.
69. Kwon, M. Y., Hong, S. Y., and Lee, K. H. (1998) *Biochim. Biophys. Acta 1387*, 239−248.
70. Martenson, R. E., Park, J. Y., and Stone, A. L. (1985) *Biochemistry 24*, 7689−7695.
71. Kawano, K., Yoneya, T., Miyata, T., Yoshikawa, K., Tokunaga, F., Terada, Y., and Iwanaga, S. (1990) *J. Biol. Chem. 265*, 15365−15367.
72. Perutz, M. F., Gronenborn, A. M., Clore, G. M., Fogg, J. H., and Shih, D. T.-B. (1985) *J. Biol. Chem. 183*, 491−498.
73. Hammond, M. S., Houliston, R. S., and Meiering, E. M. (1998) *Biochem. Cell Biol. 76*, 294−301.
74. Oishi, O., Yamashita, S., Nishimoto, E., Lee, S., Sugihara, G., and Ohno, M. (1997) *Biochemistry 36*, 4352−4359.
75. Wang, G., Sparrow, J. T., and Cushley, R. J. (1997) *Biochemistry 36*, 13657−13666.
76. Burley, S. K., and Petsko, G. A. (1986) *FEBS Lett. 203*, 139−143.
77. Lajoie, G., and Brewer, D. (2000) Cyclic Analogs of Histatins. CA 2285673, Oct 21, 1999.

BI015926D